Physics of Plasmas

Spatial symmetry breaking in single-frequency CCP discharge with transverse magnetic field

Cite as: Phys. Plasmas **25**, 080704 (2018); https://doi.org/10.1063/1.5033350
Submitted: 05 April 2018 . Accepted: 31 July 2018 . Published Online: 14 August 2018

Sarveshwar Sharma, Igor D. Kaganovich, Alexander V. Khrabrov, Predhiman Kaw, and Abhijit Sen

Spatial symmetry breaking in single-frequency CCP discharge with transverse magnetic field

Sarveshwar Sharma,[1,2,a)] Igor D. Kaganovich,[3] Alexander V. Khrabrov,[3] Predhiman Kaw,[1,b)] and Abhijit Sen[1]
[1]*Institute for Plasma Research, Bhat, Gandhinagar 382 428, India*
[2]*Homi Bhabha National Institute, Anushaktinagar, Mumbai 400 094, India*
[3]*Princeton Plasma Physics Laboratory, Princeton University, Princeton, New Jersey 08543, USA*

(Received 5 April 2018; accepted 31 July 2018; published online 14 August 2018)

An independent control of the flux and energy of ions impacting on an object immersed in a plasma is often desirable for many industrial processes such as microelectronics manufacturing. We demonstrate that a simultaneous control of these quantities is possible by a suitable choice of a static magnetic field applied parallel to the plane electrodes in a standard single frequency capacitively coupled plasma device. Our particle-in-cell simulations show a 60% reduction in the sheath width (that improves control of ion energy) and a fourfold increase in the ion flux at the electrode as a consequence of the altered ion and electron dynamics due to the ambient magnetic field. A detailed analysis of the particle dynamics is presented, and the optimized operating parameters of the device are discussed. The present technique offers a simple and attractive alternative to conventional dual frequency based devices that often suffer from undesirable limitations arising from frequency coupling and electromagnetic effects. *Published by AIP Publishing.*
https://doi.org/10.1063/1.5033350

In plasma devices used for industrial processes such as etching, surface engineering, and material deposition, the ion impact energy and the flux of ions incident on a target object are important parameters that influence the quality and throughput of the entire process. In the commonly used capacitively coupled plasma (CCP) device, typically operated by a single radio frequency (RF) source, e.g., at 13.56 MHz,[1–3] these parameters are governed by the geometry, the operating pressure, and the input power of the device. For a fixed geometry and pressure, both the ion energy and ion flux vary with the input power. Therefore, in a single frequency capacitively coupled plasma (SF-CCP) device, the ion energy and ion flux cannot be controlled independently.[4–11] To overcome this constraint, some alternate schemes have also been developed in the past. A dual-frequency device (DF-CCP)[12–16] that is now widely used in the semiconductor industry utilizes a high frequency (f_h) component to largely control the plasma density (and hence the ion flux) while a low frequency (f_l) component influences the sheath width and thereby the ion energy. However, independent control of these two parameters can get compromised if the two frequencies are too close to each other because of mutual coupling between the f_l and the f_h frequencies.[8,17–19] One way to minimize this frequency coupling is to choose f_h to be very high compared to f_l. However, for very high frequencies, say $f_h > 70$ MHz, electromagnetic effects can limit the uniformity of the reaction process.[20–22] Other alternative schemes exploit electrical asymmetry effects.[23–25]

At a fundamental level, the superiority of the DF-CCP over the SF-CCP arises from the fact that the two disparate frequencies of the former can independently influence the dynamics of the electron and ion species of the plasma. The f_h has a large influence on the electrons while the f_l acts on the ions. As is well known, such a difference in the dynamical behavior of electrons and ions can also be brought about by employing a static magnetic field of a strength such that the electrons are magnetized while the ions are not. The question is will the application of such a magnetic field parallel to the electrodes in a SF-CCP provide it with an ability to achieve simultaneous control of the ion flux and ion energy to attain the desired optimum values for a given industrial application. Our present work is devoted to exploring such a possibility by carrying out extensive particle-in-cell (PIC) simulations of a model SF-CCP with an applied static magnetic field. Magnetic fields have been employed in the past by many researchers in the area of magnetically enhanced reactive ion etching (MERIE).[28–33] Kushner[28] used a 2-D hybrid fluid simulation for an argon plasma and reported that the performance of low-pressure CCP discharges can be improved by using a transverse (parallel to substrate) static magnetic field (tens to hundreds of Gauss) to increase the plasma density. In Ref. 34, You *et al.* have experimentally studied the influence of a magnetic field on asymmetric SF-CCP argon discharges (operated at 13.56 MHz) at low and intermediate pressures. They observed a shift of the density along the electrodes arising from an $E \times B$ drift due to the electric field perpendicular to the electrodes and B parallel to the electrodes. In the IBM MERIE reactor, the magnetic field is slowly rotated in the plane parallel to electrodes to mitigate this effect. Although the MERIE process has been studied for long, the magnetic field induced asymmetry effect has escaped attention. Other recent studies devoted to CCP operation in the presence of an external magnetic field[26,27,34] have explored somewhat

a)E-mail: sarvesh@ipr.res.in.
b)Deceased.

different effects. Yang *et al.*[35,36] have used an asymmetric magnetic field with variable gradients to create asymmetry in the configuration of a CCP device. Their particle simulation studies show that the magnetic field asymmetry provides a means of independently controlling the ion flux and ion energy. They did not report any enhancement in the ion flux or efficient control of the ion energy with a weak magnetic field. Our present 1D-3V (i.e., one spatial and three velocity) PIC simulations show that such a capability can also be created in a symmetric SF-CCP discharge by application of a uniform B field. We find that for a given RF frequency, the magnitude of the central density and its location as well as the sheath width at the electrodes can be precisely controlled by the strength of the magnetic field. Therefore, by varying the magnetic field, we can control both the ion density (and hence the ion flux) and the ion energy impacting on the electrode.

Our simulations of CCP discharge have been performed with the well tested and widely used electrostatic direct implicit code EDIPIC (details can be found in Refs. 37–41). We use a simple model discharge between two plane parallel electrodes that are separated by a gap of 10 cm with a RF voltage of 1000 V and a frequency of 27.12 MHz applied to one of the electrodes (PE) while the other is grounded (GE); note that these designations are arbitrary for a 1d system and observed asymmetric structures can be inverted by changing the initial phase of the driving waveform. The choice of $L = 10$ cm, the discharge gap, is completely arbitrary and not related to any commercial plasma system. However, the electrode dimensions are assumed to be much larger than the gap distance so that a one dimensional spatial assumption holds good. Likewise, the applied voltage is chosen to be large at 1 kV keeping in mind the use of He as the working gas in our model. Compared to argon, He has a higher ionization potential and much lower ion mass requiring a higher voltage for its breakdown and sustenance. Such voltages are not unrealistic and rf voltages in the kV range are routinely used in many present day CCP processing reactors.[50–52] One of the earliest examples of a high voltage (~2 kV) He discharge is the work by Godyak and Khanneh[53] An external magnetic field (B), applied parallel to the electrodes, is varied from 0 G to 70 G. Note that although the code is one dimensional in space, it is three dimensional in velocity space so that the $E \times B$ motion of the charged particles is correctly simulated. In simulations, it is easier to assume a given potential on electrodes and allow for the current form to adjust accordingly and hence the external circuit is not included in the simulation. It should be pointed out however that the external circuit has to allow a time-averaged net current because it exists in the asymmetric state. We may also mention here that in order to test the robustness of the magnetic field induced asymmetry effects, we have carried out additional simulations using $L = 6$ cm, $B = 30$ G, and $V = 1000$ V and $L = 10$ cm, $B = 25$ G, and $V = 600$ V while keeping all other parameters the same and observed similar asymmetry effects. A uniform temperature of 300 K is assumed for the Helium gas with a typical pressure of 10 mTorr. The code calculates the time evolution of singly ionized He^+ and electrons and takes account of electron-neutral elastic[42,43] and ionization collisions[44] as well as ion-neutral elastic[45] and charge exchange collisions.[46] The metastable reactions are not considered because of the ambient low pressure. At high voltages, secondary electrons generated by either ion or electron-induced emission can modify the discharge.[47] However, for the sake of simplicity, in this paper, we only focus on the physics of the rf sheath and its modification by a weak magnetic field and neglect the generation of secondary electrons. The more complex interaction with secondary electrons will be discussed in future publications. The initial ion and electron temperatures are taken to be 0.03 eV and 2.5 eV, respectively. The number of cells is taken to be 3403, and the cell size is therefore 10 cm/3403 $\sim 2.93 \times 10^{-3}$ cm which is sufficient to resolve the electron Larmor radius of 0.22 cm at the highest magnetic field of 70 G. The cell size, Δx, is also sufficiently small to resolve the initial Debye length (λ_{de}) of 2.35×10^{-2} cm. The time step for our simulations, Δt, is taken to be 7.834×10^{-12} s to ensure that the code strictly follows the stability criterion of $\Delta x/\lambda_{de} < 0.5$ and $\omega_{pe}\Delta t < 0.2$. We take about ~400 superparticles per cell. Our simulation results, discussed next, pertain to steady state values, which is verified by comparing the derivative of the ion flux with the ionization source. Anomalous transport effects[48,49] which may be important for an overall two-dimensional structure of the discharge have been neglected in our 1-D simulations. Incorporating anomalous transport effects in a 1D simulation model is difficult without introducing artificial (non-consistent) mechanisms. Hence, for simplicity, we have restricted ourselves to considering only collisional transport effects. We do not solve the neutral gas dynamics and therefore the background gas is uniformly distributed maintaining the gas pressure at 10 mTorr. The electrodes have perfectly absorbing boundary conditions. We would also like to mention that our simulations do not take into account the matching network and blocking capacitor so that the self-bias of powered electrode is assumed to be zero.

We now discuss our simulation results. Figure 1 shows the spatial profiles of the plasma electron and ion densities, n_e and n_i, respectively, in the gap between the electrodes for

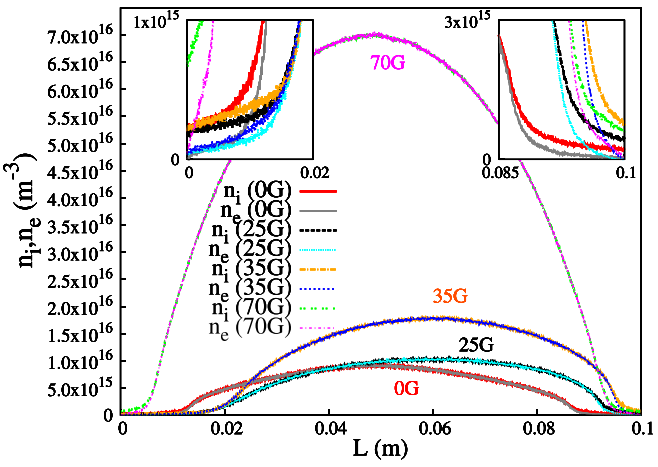

FIG. 1. Variation of the time averaged spatial profiles of n_e and n_i with changes in the applied magnetic field B. The insets show the details of the profiles near the electrodes and highlight the asymmetry of the sheath structures. The asymmetry is maximum at 35 G for fixed values of other parameters of the simulation. Here, the PE and GE are at 0 and 10 cm, respectively.

various values of B. Here, the powered electrode (PE) is at 0 cm and the grounded electrode (GE) is at 10 cm. For $B = 0$ G, the peak bulk density of $\sim 9.2 \times 10^{15}$ m^{-3} is located at the center of the discharge (5.0 cm) and the two electrode sheaths are identical with widths of 1.5 cm. The sheath width is taken to be the maximum distance from the electrode where the quasi-neutrality condition breaks down.[1] The ion and electron densities, n_i and n_e, at the left and right electrodes are 2.0×10^{14} m^{-3} and 8.0×10^{13} m^{-3}, respectively, with $n_e < n_i$. By increasing the strength of B (e.g., to 30 G), the peak value of the bulk plasma density shifts towards the GE to 6.2 cm and the density of the bulk plasma also increases up to 1.33×10^{16} m^{-3} at 30 G. An increase in the bulk density implies an increase in the ion flux. We also note that the sheath width near GE is narrow ($\sim$0.75 cm) compared to the sheath width near the PE ($\sim$1.9 cm) [see insets]. So, by controlling the sheath width (through B), we can control the potential drop across it and hence the ion energy. We also find that n_i at PE (2.1×10^{14} m^{-3}) is nearly 3 times less than that at GE (6.25×10^{14} m^{-3}) and $n_e > n_i$ at PE ($n_e \sim 2.6 \times 10^{14}$ m^{-3}) during a short interval of an RF cycle. At GE, $n_i > n_e$ but curiously $n_e - n_i$ does not go to a minimum at the end of the RF cycle which is at variance from the behavior in a normal single frequency CCP discharge. At $B = 35$ G, the sheath width near GE is 0.6 cm, and at PE, it is 1.71 cm. The center of the bulk plasma is at $\sim$6.2 cm. Here, n_i at GE ($\sim 8.0 \times 10^{14}$ m^{-3}) is more than 3 times higher compared to that at PE ($\sim 2.5 \times 10^{14}$ m^{-3}). Again, like the 30 G case, n_e ($\sim 3.1 \times 10^{14}$ m^{-3}) at PE is higher than n_i ($\sim 2.5 \times 10^{14}$ m^{-3}) and at GE ($\sim 3.0 \times 10^{13}$ m^{-3}) is nearly 25 times lower than n_i ($\sim 8.0 \times 10^{14}$ m^{-3}), which is a very unusual phenomenon since in general $n_i > n_e$ at the electrodes in normal CCP discharges. This unusual phenomenon is attributed to the strange shape of the potential profile existing over a short duration of an RF period. We will discuss the physical reason for this abnormal behavior later in the text. By increasing B (from 40 G to 70 G), the density of the bulk plasma increases and the center of the peak density shifts towards PE. Finally, at 70 G, the center of peak density is at 5 cm and both sheaths are again nearly symmetric with a sheath width of $\sim$0.8 cm. The ion density at both the right and left electrodes is $\sim 6.5 \times 10^{14}$ m^{-3}, and the electron density is $\sim 2.0 \times 10^{14}$ m^{-3}, i.e., $n_i > n_e$ which is similar to the $B = 0$ G case. The sheath width at 70 G is less compared to that at 0 G ($\sim$1.5 cm) because the density in the former case ($\sim 7.0 \times 10^{16}$ m^{-3}) is nearly 8 times high compared to that in the latter case ($\sim 9.0 \times 10^{15}$ m^{-3}).

Figure 2 shows the rate of volume ionization [$Z(x)$], ion current density (J_i), electron current density (J_e), and ion energy (E_i) corresponding to three different phases (i.e., 0, π, and $3\pi/2$) of the applied potential (V) during an RF cycle for the 35 G case. Here, the time averaged ion energy (local, per particle) in the steady state is about $\sim$2.1 eV and the corresponding ion Larmor radius is $\sim$8.5 cm. In this figure, the values of V at the powered electrode for the panels [(a) and (b)], [(c) and (d)], and [(e) and (f)] are –1000 V, 1000 V, and –100 V, respectively. $Z(x)$ is nearly uniform at 0 G but becomes nonuniform and shifts towards the powered electrode when B is increased. The magnitude of ionization rate

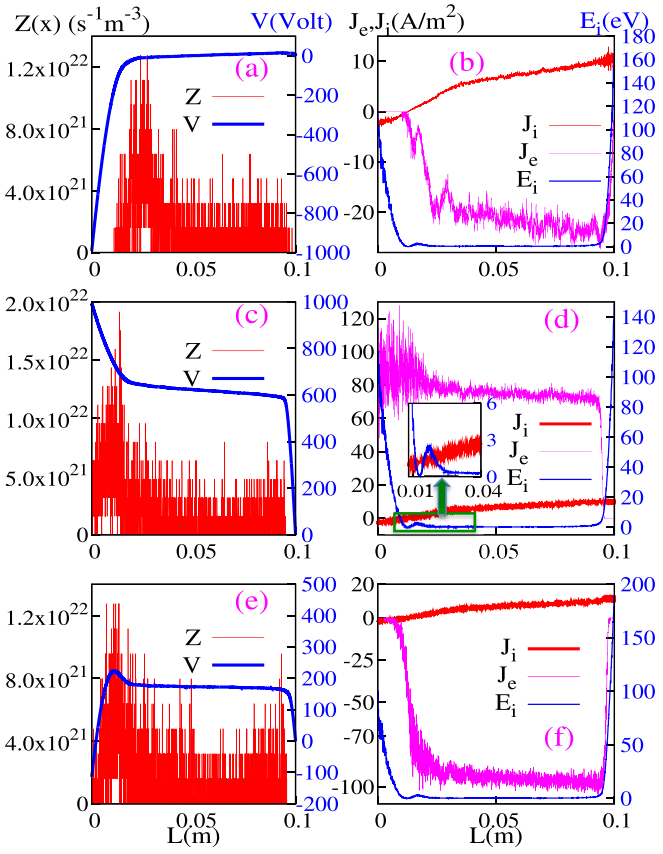

FIG. 2. Spatial profiles of potential (V), rate of volume ionization [$Z(x)$], ion current density (J_i), electron current density (J_e), and ion energy (E_i) for three different phases of V during an RF cycle for $B = 35$ G. The inverted potential profile seen in (c) confines the ions and accelerates the electrons. These accelerated electrons create an additional volume ionization peak seen in the Z(x) curves. The ion current J_i spatial profiles show a distinct asymmetry between PE and GE.

$Z(x)$ is maximal, i.e., $\sim 1.9 \times 10^{22}$ s^{-1} m^{-3} for 35 G at $x \approx 1.3$ cm. This phenomenon can be understood by looking at the profile of potential (V) in Fig. 2(c). Here, the potential difference between the PE ($x = 0$ cm) and the center of bulk plasma (i.e., $V_{PB} = V_{PE} - V_{BP}$) is $\sim$380 V and the distance over which this potential difference exists is 0 to 3 cm. A similar type of potential profile was also reported by Kushner.[28] Here, V_{PE} and V_{BP} are the potentials at PE and the center of discharge, respectively. For $B = 0$ G, the electrons become lost to the electrode and make it negatively charged leading to the development of a positive space charge ion sheath near the electrode. The potential in the bulk plasma is always higher compared to the PE. The potential drops across the sheaths accelerate the ions towards the electrodes and confine the electrons inside the bulk plasma. In general, the ions are lost continually and in equal amounts at both sheaths but the electrons are lost at both sheaths during only a small fraction of an RF period, namely, when the repelling-electrons electric field at the wall reaches its minimum (such as in the 0 G case). However, when the magnitude of B is significant (i.e., 35 G here) so that the electrons are magnetized while the ions are not, an inverted potential profile Fig. 2(c) is developed between the PE and the center of the discharge (V_{PB}). Such a phenomenon can be

understood as follows. For the $B = 0$ G case, since the ions are lost continuously and in equal amounts at both sheaths, the ion current density J_i is symmetric and equal at both electrodes ($\sim$4 A/m^2). For $B = 35$ G, the electrons do not get a chance to be lost at the GE (in an RF cycle) as the electrode sheath never collapses (the time when electrons are lost to the electrode). Under these conditions, the electrons can only be lost from the PE when the biased plate is positive with respect to the plasma [as shown in Fig. 2(c)]. Because there is a continuous loss of ions at the GE in order to conserve current, most of the electrons, which are formed due to strong ionization near the PE, are absorbed at the PE in a fraction of an RF cycle. On the other hand, the ions are pushed towards the GE by the potential V_{PB}. The ion loss rate is thus mostly towards the GE and exhibits a strong asymmetry. By observing the profile of J_i, it is clear that the ion current on the left electrode ($\sim$2 A/m^2) is much lower than that on the right electrode ($\sim$11 A/m^2). It is important to note here that the potential V_{PB} accelerates the electrons and stops the ions when the charged particles move towards the PE. These magnetized electrons accelerate under V_{PB} creating a large rate of ionization near $\sim$1.25 cm which is nearly 4 times higher than the 0 G case. The PE absorbs the electrons generated due to ionization, and the ions are pushed back towards the GE. The ion acceleration can be identified in Fig. 2 where the ion energy E_i is seen to increase from $\sim$1.25 cm to 2.2 cm which is higher than the E_i from 5.0 cm to $\sim$9.0 cm (up to the sheath edge near the GE).

We have also measured the time evolution of the electric field [E (V/m)] at both the PE and the GE for 0 G and 35 G cases. At 0 G, only the magnitude of E changes at both electrodes (due to expansion and collapse of the electron sheath). Conversely, at 35 G, the electric field at GE just changes its magnitude (like 0 G) but at the PE, E (magnitude of E at PE is much higher compared to that of E at GE) not only changes its magnitude but also changes its direction for a short interval of time (due to V_{PB}).

The physical consequences of the changed dynamics of electrons and ions continue to be interesting when B is further increased to 70 G. Here, electrons are strongly magnetized and ions are weakly magnetized. As shown in Fig. 3, the magnitude of $Z(x)$ is almost symmetric between both sides from the center of discharge. It is maximum near the sheath edges ($\sim 1.6 \times 10^{22}$ s^{-1}m^{-3}) and is nearly uniform ($\sim 6.0 \times 10^{21}$ s^{-1}m^{-3}) elsewhere. Again, this phenomenon can be understood by observing the profile of the potential (V) in Fig. 3(c). Here, the potential difference between the PE and the center of bulk plasma (i.e., $V_{PB} = V_{PE} - V_{BP}$) is $\sim$130 V, which is nearly 3 times less compared to $B = 35$ G. Furthermore, the length in which this potential difference has been developed is 0.65 cm that is nearly 5 times less compared to the 35 G case. So, it is clear that for $B = 70$ G, the electrons are not only accelerated by a smaller V_{PB} but also for a very short distance (0.65 cm) near to both electrodes which makes the ionization profile symmetric with respect to the center of bulk plasma. The magnitude of $Z(x)$ is also lower compared to the 35 G case. Also, this V_{PB} at 70 G is not strong enough to stop the majority of ions when they move towards the PE. A curious feature, observed for

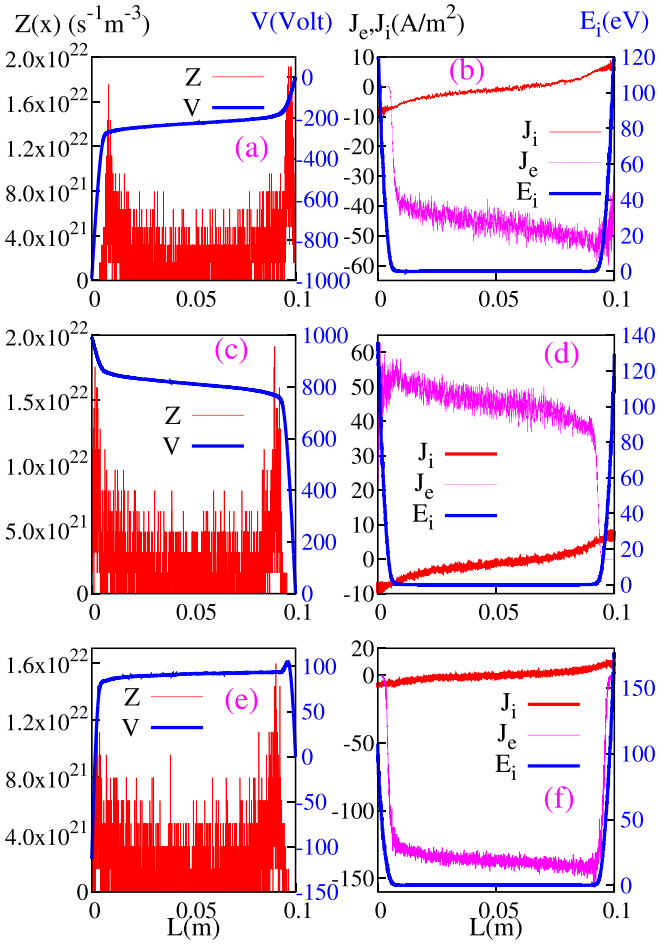

FIG. 3. Spatial profiles of V, $Z(x)$, J_i, J_e, and E_i for three different phases of V during an RF cycle for $B = 70$ G. At this higher value of the magnetic field, the magnitude of the inverted potential profile decreases and the ionization profile starts to become symmetric again with respect to the center of discharge. The ion current profile also becomes symmetric.

the high magnetic field case and that arises from the changed mobility of the electrons, is the development of an inverse sheath in front of both the PE and the GE. This can be clearly seen from Figs. 3(a) and 3(c) and is a phenomenon that needs to be explored in more depth in the future.

As remarked earlier, for $B = 0$ G, the potential in the bulk plasma is always higher (or positive with respect to the ground) than that at GE. However, it is surprising that for $B = 70$ G, the bulk potential is lower (i.e., negative) with respect to the GE for a short time when V at the powered electrode is –1000 V [see Fig. 3(a)]. The potential V at the PE is also slightly higher than the bulk potential when V approaches 1000 V. This is indicative of an interesting result, namely, the existence of an electron-rich sheath near the GE and PE during a short interval of an RF period.

For the $B = 0$ G case, the ions are lost equally and continually from both the sheaths, but the electrons are lost from both the sheaths during a fraction of an RF period when the electron sheath edge reaches a minimum distance from the electrodes. However, at 70 G, the potentials V_{PB} at the powered and V_{GB} at the grounded electrode accelerate the electrons and have a negligible effect on the ion motion when the charge particles move towards the electrodes. Here, V_{GB}

is the potential difference between the GE and the bulk plasma [see Fig. 3(a)]. The ions are lost at both electrodes continuously; however, electrons are collected by both PE and GE alternatively during short intervals of an RF cycle.

Like in the unmagnetized case, at 70 G, J_i is symmetric and equal at both electrodes ($\sim$7 A/m^2). The GE and PE are positive [see Figs. 3(a) and 3(c)] with respect to the bulk plasma during a small interval of an RF cycle. During this particular phase of an RF cycle, the electrons are pulled in by both the electrodes alternatively due to V_{GB} and V_{PB} [see profile of J_e in Figs. 3(b) and 3(d)]. The profile of ion energy E_i [Figs. 3(b), 3(d), and 3(f)] shows that the ions flow smoothly as in the unmagnetized case.

We have also measured the time evolution of E (V/m) at both PE and GE for $B = 70$ G and found that it not only changes its magnitude but also changes its direction for short intervals of time (due to V_{GB} and V_{PB}).

It is important to point out at this stage that the asymmetry effect in the sheaths can also be influenced by other operating parameters of the device, such as the applied frequency, the pressure, the applied voltage, and the type of gas. To highlight one such influence, we have studied the applied frequency effect by repeating our simulations at different values of B over a range of frequencies, namely, 13.56 MHz, 27.12 MHz, and 60 MHz. The changes in the ion flux (Γ_i) and in the ion energy (E_i) at GE for three different frequencies are shown in Fig. 4. The dotted ellipticals are drawn to highlight the fact that at a particular frequency, one can get maximum ion flux with minimum ion energy for an appropriate choice of the magnetic field strength. Here, Γ_i at 13.56 MHz is small compared to the ion fluxes at other frequencies. We see that for chosen specific values of B, it is possible to get a maximum in Γ_i and a minimum in E_i simultaneously in each case. For 13.56 MHz at 25 G, the maximum of Γ_i is 3.0×10^{19} m^{-2}s^{-1} and the minimum E_i is 130 eV. Similarly, for 27.12 MHz (at 35 G) and 60 MHz (at 18 G), the maximum values of Γ_i are 6.7×10^{19} m^{-2} s^{-1} and 1.1×10^{20} m^{-2} s^{-1}, respectively, while the minimum values of E_i are 140 eV and 342 eV, respectively. Likewise, variations in other basic parameters such as pressure, applied voltage, or type of gas in the presence of a magnetic field reveal a rich operating space for the SF-CCP where high ion flux with a simultaneous control of ion energy can be achieved. Details

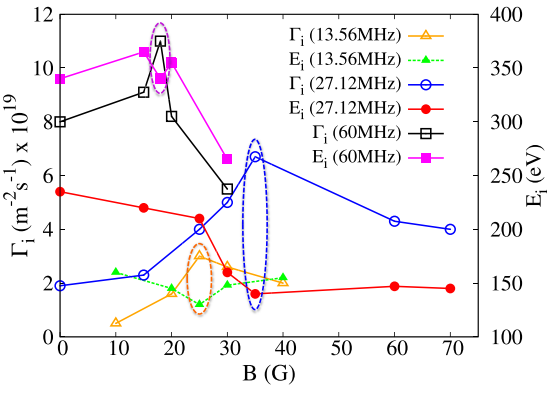

FIG. 4. Variation of Γ_i and E_i at the grounded electrode as a function of B for 3 different applied frequencies.

of these additional simulations will be reported in follow-up publications.

In summary, our simulations provide a proof-of-principle demonstration of the effective use of a static magnetic field to significantly improve the operating characteristics of a standard CCP and thereby provide a simple alternative technique to simultaneously control the ion flux and ion energy in such devices. The basic physical mechanism underpinning this control is the altered dynamics of the electrons and ions under the influence of the magnetic field that impacts the location and magnitude of the ionization region as well as the width of the sheaths at the electrodes. The magnitude of the magnetic field is chosen to be such that the electrons are strongly magnetized resulting in their reduced mobility across the magnetic field while the ions remain relatively unmagnetized. It is then possible to optimize the operating parameters of the device in a desired manner by a suitable choice of the other basic parameters of the device. Our simulations have been carried out for physically realistic values of plasma parameters (a low pressure He discharge) and a magnetic field of $\sim$35 G that can be easily recreated in a laboratory setup to experimentally test the basic concept. In an actual experiment, deviations from our simulation results are likely to arise due to the limitations of our model calculations such as the one dimensional approximation, unavoidable non-uniformity in the magnetic field, assumption of a constant voltage operation rather than a constant power operation, etc. However, it is hoped that our present findings can become the basis for both further numerical simulations (2d and 3d) and experimental explorations of this concept in order to assess the feasibility of a practical device exploiting this technique.

The authors would like to thank Shali Yang for her help in cross-checking some of our simulation results on another PIC/MCC code (iPM).

[1]M. A. Lieberman and A. J. Lichtenberg, *Principles of Plasma Discharges and Materials Processing* (Wiley, NJ, 2005).
[2]U. Buddemeier, U. Kortshagen, and I. Pukropski, Appl. Phys. Lett. **67**, 191 (1995).
[3]L. Xu, L. Chen, M. Funk, A. Ranjan, M. Hummel, R. Bravenec, R. Sundararajan, D. J. Economou, and V. M. Donnelly, Appl. Phys. Lett. **93**, 261502 (2008).
[4]M. A. Lieberman, IEEE Trans. Plasma Sci. **16**, 638 (1988).
[5]V. A. Godyak, Sov. J. Plasma Phys. **2**, 78 (1976).
[6]O. A. Popov and V. A. Godyak, J. Appl. Phys. **57**, 53 (1985).
[7]I. D. Kaganovich, Phys. Rev. Lett. **89**, 265006 (2002).
[8]E. Kawamura, M. A. Lieberman, and A. J. Lichtenberg, Phys. Plasmas **13**, 053506 (2006).
[9]I. D. Kaganovich, O. V. Polomarov, and C. E. Theodosiou, IEEE Trans. Plasma Sci. **34**, 696 (2006).
[10]S. Sharma and M. M. Turner, Plasma Sources Sci. Technol. **22**, 035014 (2013).
[11]S. Sharma, S. K. Mishra, and P. K. Kaw, Phys. Plasmas **21**, 073511 (2014).
[12]H. H. Goto, H. D. Lowe, and T. Ohmi, IEEE Trans. Semicond. Manuf. **6**, 58 (1993).
[13]J. Robiche, P. C. Boyle, M. M. Turner, and A. R. Ellingboe, J. Phys. D: Appl. Phys. **36**, 1810 (2003).
[14]P. C. Boyle, A. R. Ellingboe, and M. M. Turner, J. Phys. D: Appl. Phys. **37**, 697 (2004).
[15]S. Sharma and M. M. Turner, J. Phys. D: Appl. Phys. **46**, 285203 (2013).

[16]S. K. Karkari, A. R. Ellingboe, and C. Gaman, Appl. Phys. Lett. **93**, 071501 (2008).
[17]J. Schulze, T. Gans, D. O'Connell, U. Czarnetzki, A. R. Ellingboe, and M. M. Turner, J. Phys. D: Appl. Phys. **40**, 7008 (2007).
[18]M. M. Turner and P. Chabert, Phys. Rev. Lett. **96**, 205001 (2006).
[19]T. Gans, J. Schulze, D. O'Connell, U. Czarnetzki, R. Faulkner, A. R. Ellingboe, and M. M. Turner, Appl. Phys. Lett. **89**, 261502 (2006).
[20]M. A. Lieberman, J. P. Booth, P. Chabert, R. J. Mand, and M. M. Turner, Plasma Sources Sci. Technol. **11**, 283 (2002).
[21]A. Perret, P. Chabert, J. P. Booth, J. Jolly, J. Guillon, and Ph. Auvray, Appl. Phys. Lett. **83**, 243 (2003).
[22]A. Perret, P. Chabert, J. Jolly, and J. P. Booth, Appl. Phys. Lett. **86**, 021501 (2005).
[23]U. Czarnetzki, J. Schulze, E. Schungel, and Z. Donko, Plasma Sources Sci. Technol. **20**, 024010 (2011).
[24]D. J. Economou, J. Vac. Sci. Technol. A **31**, 050823 (2013).
[25]T. Lafleur, Plasma Sources Sci. Technol. **25**, 013001 (2016).
[26]J. Trieschmann, M. Shihab, D. Szeremley, A. E. Elgendy, S. Gallian, D. Eremin, R. P. Brinkmann, and T. Mussenbrock, J. Phys. D: Appl. Phys. **46**, 084016 (2013).
[27]I. I. Zadiriev, A. A. Rukhadze, E. A. Kralkina, K. V. Vavilin, V. B. Pavlov, and V. P. Tarakanov, Tech. Phys. **61**(11), 1603 (2016).
[28]M. J. Kushner, J. Appl. Phys. **94**, 1436 (2003).
[29]K. P. Muller, F. Heinrich, and H. Mader, Microelectron. Eng. **10**, 55 (1989).
[30]A. V. Vasenkov and M. J. Kushner, J. Appl. Phys. **95**, 834 (2004).
[31]M. A. Lieberman and A. J. Lichtenberg, IEEE Trans. Plasma Sci. **19**, 189 (1991).
[32]D. A. W. Hutchinson, M. M. Turner, R. A. Doyle, and M. B. Hopkins, IEEE Trans. Plasma Sci. **23**, 636 (1995).
[33]J.-C. Park and B. Kang, IEEE Trans. Plasma Sci. **25**, 499 (1997).
[34]S. J. You, T. T. Hai, M. Park, D. W. Kim, J. H. Kim, D. J. Seong, Y. H. Shin, S. H. Lee, G. Y. Park, J. K. Lee, and H. Y. Chang, Thin Solid Films **519**, 6981 (2011).
[35]S. Yang, Y. Zhang, H. Wang, J. Cui, and W. Jiang, Plasma Processes Polym. **14**, 1700087 (2017).
[36]S. Yang, L. Chang, Y. Zhang, and W. Jiang, Plasma Sources Sci. Technol. **27**, 035008 (2018).
[37]D. Sydorenko, "Particle-in-cell simulations of electron dynamics in low pressure discharges with magnetic fields," Ph.D. thesis (University of Saskatchewan, Canada, 2006).
[38]M. D. Campanell, A. V. Khrabrov, and I. D. Kaganovich, Phys. Plasmas **19**, 123513 (2012).
[39]J. P. Sheehan, N. Hershkowitz, I. D. Kaganovich, H. Wang, Y. Raitses, E. V. Barnat, B. R. Weatherford, and D. Sydorenko, Phys. Rev. Lett. **111**, 075002 (2013).
[40]M. Campanell and H. Wang, Appl. Phys. Lett. **103**, 104104 (2013).
[41]J. Carlsson, A. Khrabrov, I. Kaganovich, T. Sommerer, and D. Keating, Plasma Sources Sci. Technol. **26**, 014003 (2017).
[42]M. J. Brunger, S. J. Buckman, L. J. Allen, I. E. McCarthy, and K. Ratnavelu, J. Phys. B: At., Mol. Opt. Phys. **25**, 1823 (1992).
[43]W. C. Fon, K. A. Berrington, and A. Hibbert, J. Phys. B: At., Mol. Opt. Phys. **14**, 307 (1981).
[44]D. Rapp and P. Englander-Golden, J. Chem. Phys. **43**, 1464 (1965).
[45]A. V. Phelps, J. Appl. Phys. **76**, 747 (1994).
[46]B. M. Smirnov, *Theory of Gas Discharge Plasma* (Springer, 2015).
[47]A. V. Khrabrov, I. D. Kaganovich, P. L. G. Ventzek, A. Ranjan, and L. Chen, Plasma Sources Sci. Technol. **24**, 054003 (2015).
[48]G. J. M. Hagelaar and N. Oudini, Plasma Phys. Controlled Fusion **53**, 124032 (2011).
[49]F. Gaboriau, R. Baude, and G. J. M. Hagelaar, Appl. Phys. Lett. **104**, 214107 (2014).
[50]V. A. Godyak, R. B. Piejak, and B. M. Alexandrovich, Phys. Rev. Lett. **68**, 40 (1992).
[51]V. A. Godyak, R. B. Piejak, and B. M. Alexandrovich, Plasma Sources Sci. Technol. **1**, 36 (1992).
[52]V. A. Godyak and R. B. Piejak, Phys. Rev. Lett. **65**, 996 (1990).
[53]V. A. Godyak and A. S. Khanneh, IEEE Trans. Plasma Sci. **14**, 112 (1986).